Geophysical Research Letters

RESEARCH LETTER
10.1029/2018GL080845

The Effect of Foehn-Induced Surface Melt on Firn Evolution Over the Northeast Antarctic Peninsula

Rajashree Tri Datta[1,2,3,4], Marco Tedesco[4,5], Xavier Fettweis[6], Cecile Agosta[7,8], Stef Lhermitte[8], Jan T. M. Lenaerts[9], and Nander Wever[9]

[1]Earth System Science Interdisciplinary Center, University of Maryland, College Park, MD, USA, [2]NASA Goddard Space Flight Center, Greenbelt, MD, USA, [3]The Graduate Center, CUNY, New York, NY, USA, [4]Lamont-Doherty Earth Observatory of Columbia University, Palisades, New YorkNY, USA, [5]NASA Goddard Institute of Space Studies, New York, NY, USA, [6]Department of Geography, Université de Liège, Liège, Belgium, [7]CNRS, Institut des Géosciences de l'Environnement, Université Grenoble Alpes, Grenoble, France, [8]Department of Geoscience and Remote Sensing, Delft University of Technology, Delft, Netherlands, [9]Department of Atmospheric and Oceanic Sciences, University of Colorado Boulder, Boulder, CO, USA

Key Points:
- A long-term record of foehn-induced melt is calculated from a regional climate model via two methods
- We introduce the Foehn Index which captures foehn intensity over space and time
- Late-season foehn-induced melt between 2015 and 2017 produced compounded densification in the upper snowpack resulting in increasing runoff

Supporting Information:
- Supporting Information S1

Correspondence to:
R. T. Datta,
tri.datta@gmail.com

Citation:
Datta, R. T., Tedesco, M., Fettweis, X., Agosta, C., Lhermitte, S., Lenaerts, J. T. M., & Wever, N. (2019). The effect of Foehn-induced surface melt on firn evolution over the northeast Antarctic peninsula. *Geophysical Research Letters*, *46*. https://doi.org/10.1029/2018GL080845

Received 9 OCT 2018
Accepted 4 FEB 2019

Abstract Surface meltwater ponding has been implicated as a major driver for recent ice shelf collapse as well as the speedup of tributary glaciers in the northeast Antarctic Peninsula. Surface melt on the NAP is impacted by the strength and frequency of westerly winds, which result in sporadic foehn flow. We estimate changes in the frequency of foehn flow and the associated impact on snow melt, density, and the percolation depth of meltwater over the period 1982–2017 using a regional climate model and passive microwave data. The first of two methods extracts spatial patterns of melt occurrence using empirical orthogonal function analysis. The second method applies the *Foehn Index*, introduced here to capture foehn occurrence over the full study domain. Both methods show substantial foehn-induced melt late in the melt season since 2015, resulting in compounded densification of the near-surface snow, with potential implications for future ice shelf stability.

Plain Language Summary Surface melt and the ponding of water on the surface has been linked to recent ice shelf collapse in the northeast Antarctic Peninsula, which includes the Larsen C ice shelf, one of the regions in Antarctica that is most vulnerable to a changing climate. Melt can be caused either by high temperatures or by foehn winds, that is, a hot, dry wind on the downwind side of a mountain range. To determine when foehn winds occurred from 1982 to 2017, and how much surface melt they produced, we use two methods. The first method finds recurring patterns of melt on the northeast Antarctic Peninsula from both satellite observations and models and determines which patterns are produced by foehn conditions. The second method uses simulated atmospheric conditions to determine when and over how much surface area foehn conditions occur and then calculates the melt produced at the same time. Both methods find high levels of foehn-induced melt after the summer melt season occurring since 2015, resulting in high-density snow near the surface in regions where foehn winds are common. If similar conditions persist into the future, late-season and autumn melt could have substantial ramifications for the health of the Larsen C ice shelf.

1. Introduction

Surface melt on the northeast Antarctic Peninsula (NAP) impacts the mass balance of grounded ice as well as ice shelf stability (Barrand et al., 2013; Kunz et al., 2012; Scambos et al., 2004). Besides producing meltwater runoff on the grounded part of the NAP (Hock et al., 2009), surface melt can indirectly lead to ice loss through the process of ice shelf hydrofracture, whereby preexistent crevasses on floating ice shelves fill with accumulating meltwater, leading to the ice shelf disintegration and tributary glacier speedup and thinning (Glasser & Scambos, 2008; MacAyeal & Sergienko, 2013; Rott et al., 1998, 2011; Scambos et al., 2000, 2004; van der Veen, 1998; Vaughan & Doake, 1996; Weertman, 1973). The potential contribution to global sea level rise from tributary glaciers resulting from the removal of the Larsen C ice shelf (LCIS) has been estimated at <2.55 to 2,100 mm and <4.2 to 2,300 mm (Schannwell et al., 2018).

The fate of surface meltwater, that is, meltwater in the first meter of the snowpack, depends on the conditions of underlying firn. Anomalously low accumulation, enhanced firn compaction, liquid water

percolation, and/or refreezing can all lead to firn air depletion (Kuipers-Munneke et al., 2014), in turn limiting additional meltwater storage and promoting hydrofracture. While the surface of the LCIS was found to be lowering due to a combination of surface melt and basal melt into the early part of this century (Holland et al., 2015; Pritchard et al., 2012; Shepherd et al., 2003), surface height has increased since 2009 due to reduced surface melt (Adusumilli et al., 2018), estimated at a loss of 1–2 days in melt duration from 1999 to 2017 (Bevan et al., 2018).

While the annual mean temperature over the NAP is 3–5 °C lower than over the western AP at the same latitude (Morris & Vaughan, 2003; Van Wessem et al., 2015), strong melt pulses can be produced by the foehn effect (Luckman et al., 2014), an episodic warm, dry air flow on the lee slopes of the NAP (Elvidge & Renfrew, 2016). Studies focusing on the 2010–2011 summer have calculated foehn frequencies of 20% in January to March (King et al., 2017) or 30% from November to March (Luckman et al., 2014). Observations in other seasons have found that foehn is more prevalent in winter and spring (Wiesenekker et al., 2018) and that 23% of the annual melt actually occurred in winter (Kuipers Munneke et al., 2018). Recent years (2015–2017) have shown a series of strong, late-season foehn-induced surface melt events (Bozkurt et al., 2018; Kuipers Munneke et al., 2018; Wiesenekker et al., 2018). However, due to the limited spatial and temporal coverage of contemporaneous atmospheric, surface melt, and firn records, it remains unclear how widespread these events are and how they influence snowpack conditions. Regional climate models that couple an atmospheric model with a firn model provide a useful tool to address this question.

In this study, we use output of the Modèle Atmosphérique Régionale (MAR) regional climate model v3.9 at a 7.5-km resolution as well as remote sensing microwave observations to present a long-term (1982–2017), spatially comprehensive, record of foehn intensity, surface melt, and firn conditions over the NAP. Empirical orthogonal functions (EOFs) analysis allows us to capture the primary spatial patterns (modes) of surface melt occurrence and compare modeled patterns to those retrieved independently from the spaceborne passive microwave (PMW) record. Composite modeled fields calculated from the EOF time series then allow us to characterize the atmospheric conditions responsible for patterns of melt occurrence that can be discerned on the surface. Subsequently, we introduce the *Foehn Index* (FI), which captures foehn occurrence over both space and time, as a complementary method that quantifies foehn-induced melt from the perspective of the near-surface atmosphere. A comparison between the two methods links large-scale atmospheric drivers to estimates for foehn at the surface. Both methods identify high foehn-induced melt in recent years in autumn (March and May) subsequent to the peak melt season (December, January, and February); this sequence of years is anomalous in the context of the long-term record. As a case study of the effects of persistent late-season foehn-induced melt, we use the concurrent modeled snowpack time series during these periods to investigate the impact of sporadic foehn-induced melt events on the firn layer.

2. Data

2.1. Regional Climate Model MAR

The MAR is an atmospheric regional climate model coupled to the Soil Ice Snow Vegetation Atmosphere Transfer scheme surface model (De Ridder & Gallée, 1998), containing the multilayer snow model Crocus (Brun et al., 1992). MAR has been evaluated extensively over Greenland (e.g., Fettweis et al., 2017) as well regions of Antarctica (Agosta et al., 2019; Amory et al., 2015). An evaluation of an earlier version of MAR (v3.6, run at a 10-km resolution) found that the model underestimates melt frequency over the NAP in comparison to satellite estimates (Datta et al., 2018). To remedy this bias, we use an updated version of MAR (v3.9), which contains updates to the cloud scheme (Fettweis et al., 2017). Figure S1 in the supporting information compares both model versions with observations over the 2004–2005 melt season, showing that melt occurrence is enhanced in the new version. Melt occurrence exceeds satellite estimates at the northern edges of the LCIS but is comparable to QuikSCAT ft3 (see section 2.2) estimates at the southwestern inlets. This suggests that while MAR v3.9 may overestimate melt in the northern LCIS, this version compares better to satellite estimates overall. A comparison of radiation budget components in both versions during December 2004 (Figures S1e–S1i) shows increased cloud cover, longwave radiation, and decreased values for all other radiation budget components. Wind direction (WD) values continues to compare well

with values with those calculated at the Larsen ice shelf autonomous weather station; the limited impact of slower modeled wind speeds on melt is discussed in Datta et al. (2018).

Daily melt occurrence estimated by MAR, for the purposes of this study, requires that total meltwater production simulated by MAR exceeds 1 mm water equivalent per day, a threshold previously applied in studies over Greenland (Franco et al., 2012). We note that the majority of meltwater is refrozen in the snowpack and does not contribute to runoff.

2.2. Remote Sensing Data

Spaceborne microwave satellite data are only weakly affected by the presence of clouds, which is useful for detecting melt occurrence over cloudy regions such as the NAP. Moreover, they provide a long historical record of surface melt occurrence (from 1972 onward), encompassing our full study period (1982–2017).

PMW sensors, here at a 25-km resolution, detect liquid water from the increase in brightness temperature (T_b) associated with the presence of liquid water (Ashcraft & Long, 2006; Mote et al., 1993; Tedesco, 2007; Ulaby & Stiles, 1980). The algorithm used in this study is a threshold-based method based on the winter mean T_b value, such that melt occurrence is determined when brightness temperatures exceed a threshold (T_c), determined by the winter mean brightness temperature (T_{winter}) and a limit (ΔT), in this case set to 30 K. This algorithm is described by Zwally and Fiegles (1994):

$$T_c = T_{winter} + \Delta T \tag{1}$$

Additionally, surface melt over the LCIS is derived from the Copernicus Sentinel-1 C-band synthetic aperture radar (SAR) data, here at 100-m resolution. The reduced backscattering coefficient of wet snow compared to dry snow/firn allows for the identification of surface melt based on satellite time series (Nagler et al., 2016). The Sentinel-1 SAR archive of descending passes over the LCIS was converted into a time series of backscatter σ_o image by implementing (i) thermal noise removal, (ii) radiometric calibration, and (iii) terrain correction using Advanced Spaceborne Thermal Emission and Reflection Radiometer (ASTER) Global Digital Elevation Model (GDEM) (Gorelick et al., 2017). The backscatter σ_o image time series were subsequently corrected for variations in incidence angle by applying a gamma (γ_o) correction (Small, 2011).

3. Materials and Methods

3.1. EOF Analysis

EOF analysis (Lorenz, 1956) is a method to associate a spatial pattern with a time series, reformatting K observations of a data vector x to a set of M vectors u (modes or principal components), whose elements are linear combinations of type x; a subset of M vectors can then capture the majority of variability in the data set in a simplified way (Wilks, 1995).

In this study, K is a daily time series of maps of sustained melt occurrence, as determined from both PMW and MAR over the period 1982–2017. Melt occurrence is calculated at the daily scale as a moving 5-day sum on the melt time series, in order to capture sustained melt at a synoptic time scale. This value is transformed into a z score, that is, the number of standard deviations (SDs) from the period (1982–2017) mean daily value with the annual cycle removed. The final modes are spatial maps. The composite values for atmospheric variables are constructed by restricting the days used to those preceding the day when an EOF mode is strong (i.e., when the PC time series value exceeds 0.03) and then subtracting each of these daily atmospheric values (excepting WD) by the 1982–2017 seasonal mean (e.g., December, January, and February for summer) in order to compute an anomaly. This allows us to capture anomalous atmospheric conditions that typically initiate a melt pattern.

3.2. Foehn Index

This method, denoted as the *FI*, constructs a single time series that expresses what areal extent of the NAP is foehn flow for what period of time. The FI is derived from simple criteria that have previously been applied to in situ weather station observations (Cape et al., 2015; Speirs et al., 2013); here we use hourly outputs from MAR at 2 m above the surface. The initiation of a foehn event (I_f) is associated with a change from a previous

time step characterized by an increase in temperature (ΔT) of 1 °C, a decrease in relative humidity (ΔRH) of 5%, and an increase in wind speed (ΔWS) of 3.5 m/s, with the further requirement that WD should be westerly (Steinhoff et al., 2014). The foehn event ceases when one of these conditions fails in reference to the hour preceding foehn initiation. Foehn hours are hours (h) of a day (d) and grid cell (g) when

$$I_f(g,d,h) = 1 \quad \text{if } \Delta T = +1^{\circ}\text{C}, \ \Delta\text{RH}<-5\%, \ \Delta\text{WS}>3.5\ \text{m/s}, \ \text{WD westerly} \tag{3}$$

The WD condition is determined by calculating the direction normal to the spine of the AP mountain range and then defining WD values 30° west or east of this value as westerly. As different sensitivities were tested with similar results, we opted to use the formula unchanged from previous literature (Steinhoff et al., 2014).

FI (in units of hr * m^2) integrates the foehn hours over the region (i.e., total grid cells G), by

$$\text{FI}(d) = \sum_{g=1}^{G}\sum_{h=1}^{24} I_f(g,d,h) \tag{4}$$

Finally, the total meltwater production coincident with foehn flow (M_t in units of G_t) is computed as the sum of total meltwater production simulated in the region (G_m) when the FI is positive.

$$M_t = \sum_{g=1}^{G_m}\sum_{d=1}^{D}\sum_{h=1}^{24} I_f(g,d,h)*M(g,d,h) \tag{5}$$

The mask (G_m), used throughout in the results to indicate where foehn winds are most common, contains those pixels where at least 2 days foehn flow has occurred consistently for more than 6 hr at any point over the 1982–2017 period during the month of January (Figure 3f), that is, the month when the spatial extent of foehn flow is smallest.

4. Results

4.1. Surface Melt Patterns: EOF Modes 1 and 3

Figure 1 shows the first three EOF modes from both MAR and PMW, that is, the dominant spatial patterns for sustained melt occurrence and the associated variance explained by each mode. The modeled EOF modes show substantial similarity to those computed from PMW (Figures 1a–1c vs Figures 1d–1f). EOF 1, the dominant spatial pattern showing strong melt occurrence over the whole region, explains 53% (50%) of the total variance in the time series for MAR (PMW). We determine the main atmospheric drivers associated with each EOF mode by calculating composite anomalies of modeled variables preceding strong instances of each mode as in section 3.1.

Foehn conditions are characterized by strong westerly winds leeward of the AP mountain range and a loss of moisture over the NAP, conditions that conform to conditions preceding strong EOF 1 and 3 events. Wind composites for EOFs 1 and 3 (Figures 1–1j) show anomalously high-speed winds east of the AP while near-surface RH composite anomalies show high RH west of the AP and drying to the east (Figures S2e and S2o). Cloud cover composite anomalies indicate that EOFs 1 and 3 both show cloud clearing at lower levels in the atmosphere (below 680 hPa), while only EOF 1 shows clearing persisting into higher levels in the atmosphere (i.e., above 680 hPa; Figure S2). We find that both modes are associated with high enhanced sensible heat input over the NAP that is driven by the strong turbulent mixing induced by warm westerly winds. EOF 1 is distinguished from EOF 3 by a higher net shortwave radiation anomaly and a stronger signal for each radiation balance component (Figure S3), leading to enhanced melt over the LCIS. The association of EOF 1 and EOF 3 modes with foehn flow is further corroborated by a direct comparison with the FI from 2015 to 2016 (Figure 2e and section 4.2); we find that for 78% (68%) of days when EOF 1 (EOF 3) modes are positive, the FI is greater than zero.

EOF modes associated with foehn flow (EOF 1 or EOF 3) (Figure 2a) as well as high FI values (Figure S4c) appear more prevalent prior to 2009, the turning point after which altimetry observations began to show increasing surface height over the majority of the LCIS and a decrease in western inlets (Adusumilli et al., 2018). However, in recent years, a series of high melt events (where the total melt production exceeded one SD from the monthly mean) have occurred after the climatological melt season (Figure S4b and S4d). Major melt events occurring in March and May 2016, captured in both modeled and observed EOF modes

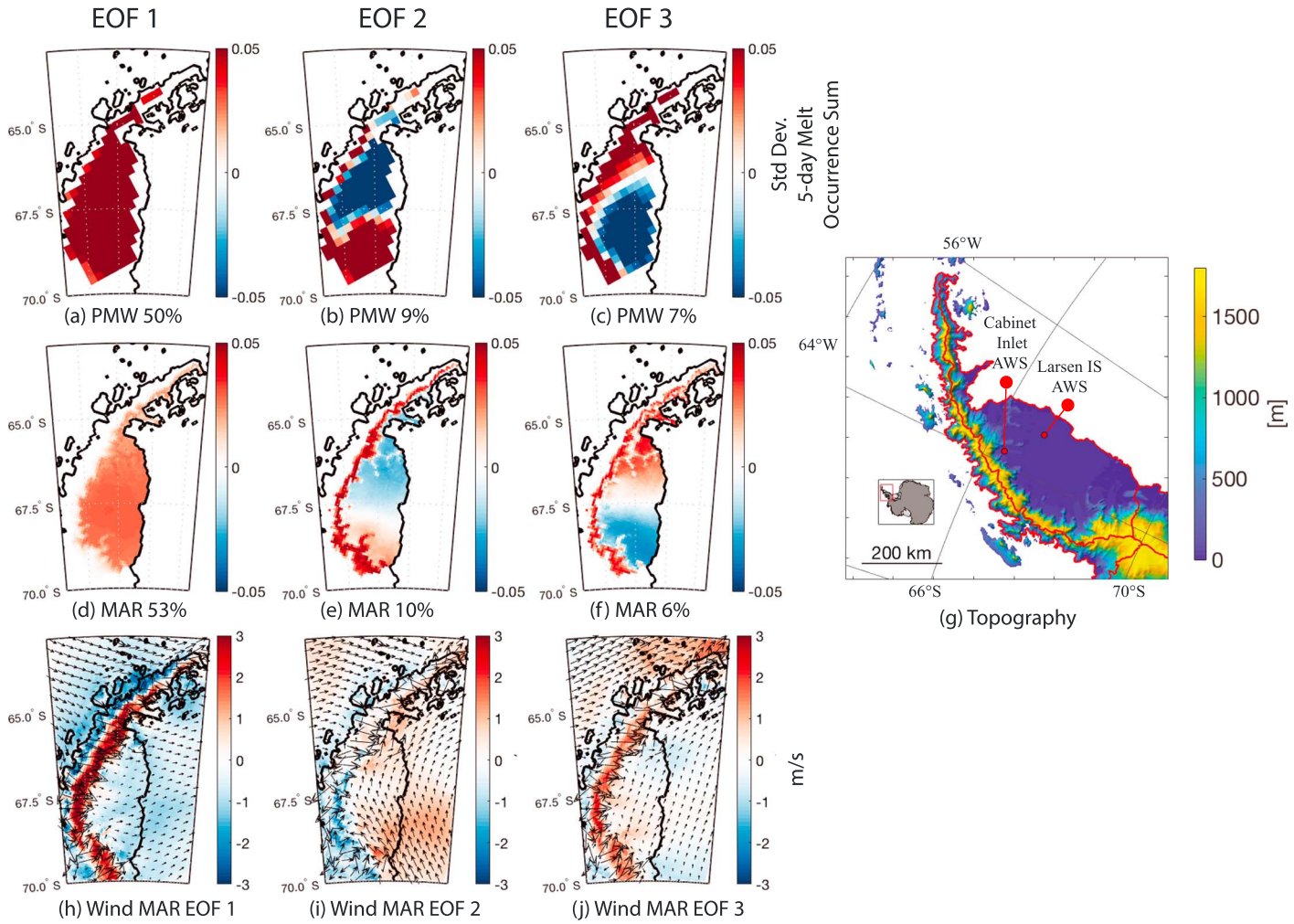

Figure 1. EOF modes (1982–2017) for (a–c) PMW and (d–f) MAR daily, shown with total variance explained for each mode (as described in the text). (h–j) Wind speed anomaly and wind direction calculated as composites when the PC time series value >0.03 for each EOF mode. PMW = passive microwave; EOF = empirical orthogonal function; MAR = Modèle Atmosphérique Régionale.

and denoted in Figure 2a and elsewhere with a pink *X* and *O*, are discussed below. (Figures 2 and S4e). EOF2, which is not associated with foehn flow, is discussed in the supporting information.

4.2. Foehn Occurrence: The FI

The FI, estimating foehn occurrence directly from near-surface atmosphere outputs over the NAP, is highest between July and September (Figure S4c), when foehn winds affect a larger surface area (Figure 2d) than they do during the summer (Figure 2c). Melt produced during increasingly warmer conditions in autumn or spring is enhanced by the more intense foehn flow typical during these seasons. The monthly mean (SD) percentage of melt concurrent with a positive FI shows a minimum of 6% (4%) in January and a maximum of 66% (15%) in September.

In recent years, meltwater production has declined in the summer months (coincident with low FI) and increased during autumn, when the FI is high. Overall meltwater production in the NE basin during December and January before 2009 was higher (averaging 27 ± 10 Gt) than in years after 2009 (averaging 16 ± 7 Gt), although the FI remained within one SD of the mean post-2009. We find that during anomalous late-season melt events (March 2015–2017 and May 2016), values for total meltwater production, FI values, and meltwater produced concurrent with a positive FI, all neared or substantially exceeded 1 SD of the monthly mean (Figures S4b–S4d). We note that the meltwater produced basin wide during May 2016

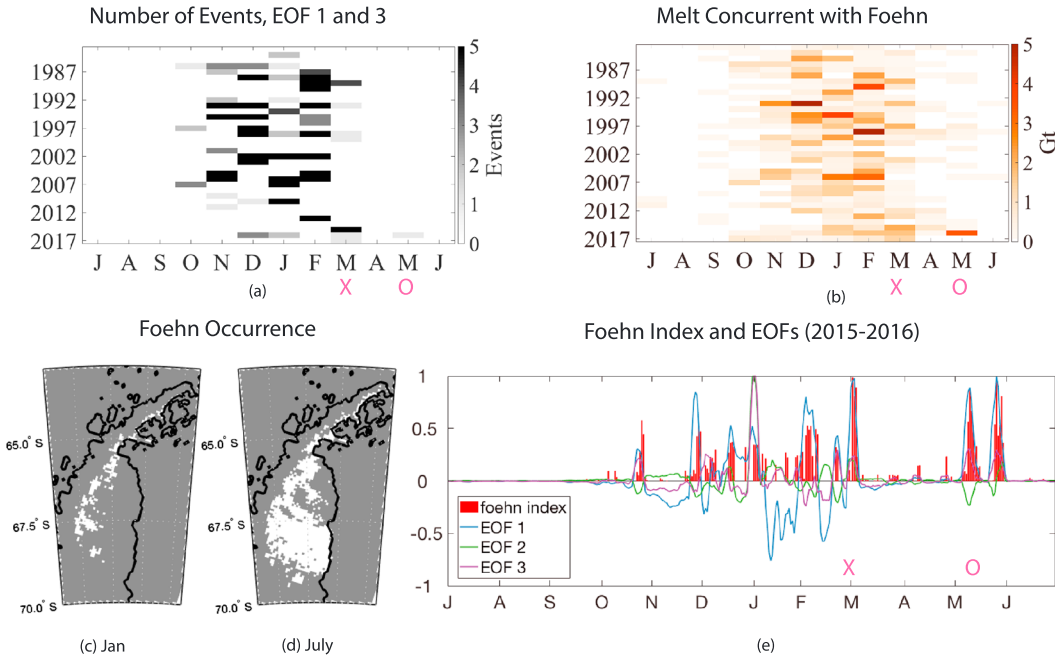

Figure 2. (a) Number of strong EOF occurrences/month, 1982–2017 period (i.e. pc > 0.03). (b) Meltwater production in the NE basin concurrent with a positive foehn index. (c, d) Regions shown in white where more than two instances of sustained foehn flow have occurred over the given month over the 1982–2017 period (G_m). (e) Normalized values for the foehn index and PC time series for EOF 1–3 over the 2015–2016 period from July to June. X,O indicate March 2016 and May 2016 melt events. EOF = empirical orthogonal function.

exceeds meltwater production in any February or March since 2009 (Figure S4a). In the following sections, we use the 2015–2017 period as a case study for the effects of compounded autumn melt events on the snowpack.

4.3. Foehn-Induced Melt From 2015 to 2016 and the Effect on the Snowpack

Sentinel SAR data, available at a spatial resolution high enough to capture even limited foehn-induced melt, confirm high melt occurrence in the G_m region during the March 2016 and May 2016 periods. (Figures 3a and 3f). Concurrent model outputs show anomalously high meltwater production due to the intrusion of westerly winds with limited blocking flow for both events, with a stronger wind and temperature signature shown in May (Figure S5). The May 2016 event is characterized by anomalously high surface density at the northern edges of the LCIS (Figures 3j and 3m). During this period, we find that meltwater percolation depth, that is, the maximum depth at which volumetric liquid water content exceeds 4%, exceeds 2-m depth for substantial portions of the western edge of the ice shelf (Figures 3k and 3n). We find that March 2016 melt event showed less melt production (Figures 3b and 3e) as well as shallower meltwater percolation (Figures 3d and 3g) than the May 2016 event.

4.4. Temporal Evolution of the Snowpack, 2015–2017

To understand the cumulative effect of late-season melt anomalies leading into the 2016–2017 melt season, we map properties of the snowpack as vertical profiles averaged over the G_m region (Figure 2c) for daily averages from July 2015 to July 2017 and for monthly averages over the study period. Liquid water profiles similar to the March events within 2015–2017 are found in 1988, 1993, and 1997 (Figure 4e) but have never previously occurred in succession of years. The May 2016 event is unprecedented, during which the percolation of liquid water exceeded a 2-m depth (Figure 4f). During the 2016–2017 melt season, we find limited liquid water present at substantial depths (Figures 4b, 4e, and 4f), unlike the 2015–2016 season (Figure 4a). By January of 2017, and unlike previous January profiles, nearly all liquid water is retained at the top of the snowpack (Figure S6a) and volumetric liquid water content exceeds 4% in only the first 0.3 m in the majority of the G_m region.

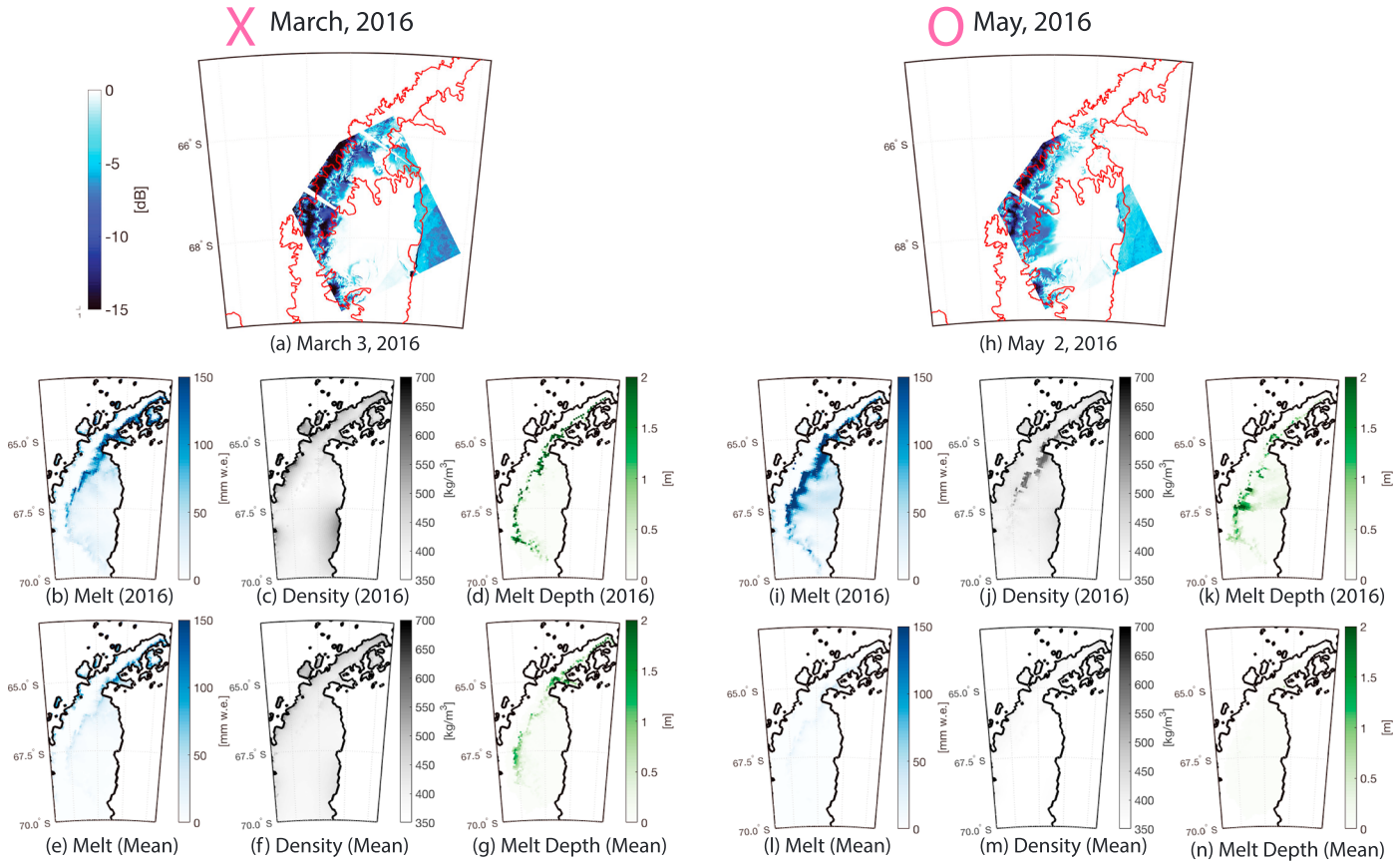

Figure 3. Six-day composite Sentinel radar backscatter (dB) estimates around (a) 3 March 2016 (h) 2 May 2016. Coastlines/grounding lines provided from MODIS, Mosaic of Antarctica (2004). Shown are the 2016 and mean meltwater production for March (b, e), May (i, l), snowpack density for March (c, f), May (j, m), and maximum snowpack depth where liquid water content exceeded 4% for March (d, g) and May (k, n). MODIS = Moderate Resolution Imaging Spectroradiometer.

Due to higher viscosity of wet snow and refreezing, the presence of liquid water has a substantial impact on density in the upper layer (Figures 4c, 4d, and S6b–S6d). While January profiles in previous years were comparable to those of 2016 (Figure S6b), the winter (July) 2016 density profile, following the melt event in May, showed anomalously high density in the upper level snowpack (i.e., above 0.4 m; Figure S6d).

From 2015 to 2017, the compounding densification due to late-season melt reduced the capacity for additional refreeze in the modeled firn layer, resulting in enhanced runoff. Modeled meltwater production in the G_m region during March of 2015–2017 exceeded 250% of the climatological average for March but showed a decreasing trend for meltwater production (300%, 220%, and 190%, respectively) and refreeze (240%, 220%, and 190%, respectively), while runoff increased (70%, 160%, and 210%, respectively). Meltwater refreezing for May 2016 comprised 1674% of the climatological average for the months.

The depletion in firn air content accompanying anomalous late-season melt reduces the capacity of firn to retain melt near the surface in the following melt season, potentially leading to deeper percolation that heats the firn column. In this version of CROCUS (Brun et al., 1992), when the snowpack reaches saturation, additional liquid water is retained in a reservoir, which can eventually be refrozen throughout the snowpack. This formulation may artificially remove meltwater in firn at the bottom of the snowpack while generating too much densification at the top. While the column model does not allow for lateral flow of water, thereby ignoring englacial or basal pathways, future work with MAR will add meltwater pathways such as evaporation and lake accumulation. Furthermore, MAR did not include the effects of blowing snow, which can lower albedo and increase surface compaction, thus enhancing the effects of foehn-induced melt on the snowpack.

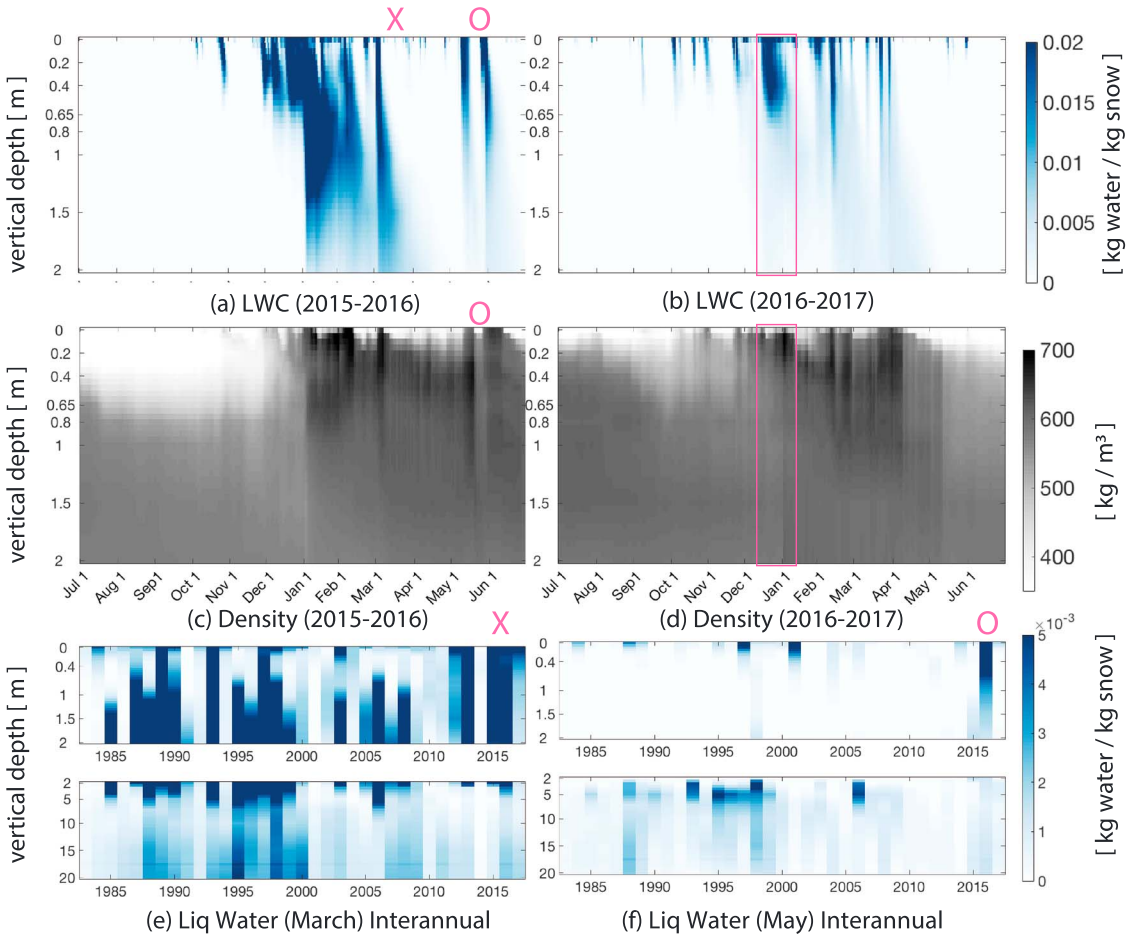

Figure 4. The effect of meltwater on the snowpack where foehn winds occur in January (mask shown in Figure 2). Mean daily liquid water content in kg water/kg snow for (a) 2015–2016 and (b) for 2016–2017. (c and d) Same as Figures 4a and 4b for snowpack density. Average monthly liquid water content (in kg water/kg snow) from 0 to 20 m into the snowpack for the 1982–2017 period for (e) May and (f) July. Note the change of scale in Figures 4e–4f.

5. Conclusions

In this study, we extract foehn-induced melt over the NAP from 1982 to 2017 using two methods applied to regional climate model outputs; EOF analysis extracts atmospheric drivers for dominant surface melt patterns while the FI is calculated based on near-surface atmosphere outputs and then used to extract concurrent melt. The seasonal frequency of FI in this study conforms to earlier work finding a fall maximum and summer minimum for foehn occurrence (Cape et al., 2015), and the modeled spatial extent for foehn flow conforms to the same cycle. In recent years, both methods show lower values for foehn-induced melt in December and confirm a substantial increase during March (2015–2017) and May 2016, which are also detected in SAR- and PMW-based estimates as well as in previous work. We use these recent events as a case study to discern the potential effect of late-season melt on the snowpack, finding that, since 2015, a series of anomalous bursts of late-season melt have produced persisting densification in the upper level of the modeled snowpack in the regions of the NAP where foehn flow is common.

Autumn and spring typically show greater intensity and spatial extent of foehn flow as well as a greater potential for firn densification. Therefore, enhanced melt events during these shoulder seasons have the potential to affect the percolation of liquid water into deeper layers and leave a lasting impact on the firn layer, even if meltwater production in the summer continues to decrease in the future. Previous work has proposed that ice shelf stability can be estimated from firn-ice concentration (Alley et al., 2018) or firn air content (Holland et al., 2011), presuming a seasonal cycle with firn air depletion during the summer

balanced by winter snowfall. Even occasional late-season melt events may therefore disproportionately affect the capacity of firn to retain liquid water and therefore ice sheet stability.

Acknowledgments
Special thanks to Peter Kuipers Munneke for valuable early feedback. Partial funding provided by National Science Foundation grant 1131973. N.W. was supported by the Swiss National Science Foundation (SNSF), grant 172299 MAR model output can be found at ftp://ftp.ldeo.columbia.edu/pub/MAR/MARv3.9_AntarcticPeninsula_7pt5km/. R. T. D. developed methods and analysis. M. T. provided mentorship. X. F. provided final MAR outputs. C. A. provided guidance on MAR over Antarctica. S. L. provided SAR data/analysis. J. T. M. L. provided substantial editing of later versions of the manuscript. N. W. provided expertise on firn processes.

References

Adusumilli, S., Fricker, H. A., Siegfried, M. R., Padman, L., Paolo, F. S., & Ligtenberg, S. R. M. (2018). Variable basal melt rates of Antarctic peninsula ice shelves, 1994–2016. *Geophysical Research Letters*, *45*, 4086–4095. https://doi.org/10.1002/2017GL076652

Agosta, C., Amory, C., Kittel, C., Orsi, A., Favier, V., Gallée, H., et al. (2019). Estimation of the Antarctic Surface Mass Balance Using the Regional Climate Model MAR (1979–2015) and Identification of Dominant Processes. *The Cryosphere*, *13*(1), 281–296. https://doi.org/10.5194/tc-13-281-2019

Alley, K. E., Scambos, T. A., Miller, J. Z., Long, D. G., & MacFerrin, M. (2018). Quantifying Vulnerability of Antarctic Ice Shelves to Hydrofracture Using Microwave Scattering Properties. *Remote Sensing of Environment*, *210*, 297–306. https://doi.org/10.1016/j.rse.2018.03.025

Amory, C., Trouvilliez, A., Gallée, H., Favier, V., Naaim-Bouvet, F., Genthon, C., et al. (2015). Comparison between Observed and Simulated Aeolian Snow Mass Fluxes in Adélie Land, East Antarctica. *The Cryosphere*, *9*(4), 1373–1383. https://doi.org/10.5194/tc-9-1373-2015

Ashcraft, I. S., & Long, D. G. (2006). Comparison of methods for melt detection over Greenland using active and passive microwave measurements. *International Journal of Remote Sensing*, *27*(12), 2469–2488. https://doi.org/10.1080/01431160500534465

Barrand, N. E., Vaughan, D. G., Steiner, N., Tedesco, M., Kuipers-Munneke, P., Van den Broeke, M. R., & Hosking, J. S. (2013). Trends in Antarctic peninsula surface melting conditions from observations and regional climate modeling. *Journal of Geophysical Research: Earth Surface*, *118*, 315–330. https://doi.org/10.1029/2012JF002559

Bevan, S. L., Luckman, A. J., Munneke, P. K., Hubbard, B., Kulessa, B., & Ashmore, D. V. (2018). Decline in surface melt duration on Larsen C ice shelf revealed by the Advanced Scatterometer (ASCAT). *Earth and Space Science*, *5*, 578–591. https://doi.org/10.1029/2018EA000421

Bozkurt, D., Rondanelli, R., Marin, J. C., & Garreaud, R. (2018). Foehn event triggered by an atmospheric river underlies record-setting temperature along continental Antarctica. *Journal of Geophysical Research: Atmospheres*, *123*, 3871–3892. https://doi.org/10.1002/2017JD027796

Brun, E., David, P., Sudul, M., & Brunot, G. (1992). A numerical model to simulate snow-cover stratigraphy for operational avalanche forecasting. *Journal of Glaciology*, *38*(128), 13–22. https://doi.org/10.1017/S0022143000009552

Cape, M. R., Vernet, M., Skvarca, P., Marinsek, S., Scambos, T., & Domack, E. (2015). Foehn winds link climate-driven warming to ice shelf evolution in Antarctica. *Journal of Geophysical Research: Atmospheres*, *120*, 11,037–11,057. https://doi.org/10.1002/2015JD023465

Datta, R. T., Tedesco, M., Agosta, C., Fettweis, X., Kuipers Munneke, P., & van den Broeke, M. R. (2018). Melting over the northeast Antarctic peninsula (1999–2009): Evaluation of a high-resolution regional climate model. *The Cryosphere*, *12*(9), 2901–2922. https://doi.org/10.5194/tc-12-2901-2018

De Ridder, K., & Gallée, H. (1998). Land surface-induced regional climate change in southern Israel. *Journal of Applied Meteorology*, *37*(11), 1470–1485. https://doi.org/10.1175/1520-0450(1998)037<1470:LSIRCC>2.0.CO;2

Elvidge, A. D., & Renfrew, I. A. (2016). The causes of Foehn warming in the lee of mountains. *Bulletin of the American Meteorological Society*, *97*(3), 455–466. https://doi.org/10.1175/BAMS-D-14-00194.1

Fettweis, X., Box, J. E., Agosta, C., Amory, C., Kittel, C., Lang, C., et al. (2017). Reconstructions of the 1900–2015 Greenland ice sheet surface mass balance using the regional climate MAR model. *The Cryosphere*, *11*, 1015–1033. https://doi.org/10.5194/tc-11-1015-2017

Franco, B., Fettweis, X., Lang, C., & Erpicum, M. (2012). Impact of spatial resolution on the modelling of the Greenland ice sheet surface mass balance between 1990–2010, using the regional climate model MAR. *The Cryosphere*, *6*, 695–711. https://doi.org/10.5194/tc-6-695-2012

Glasser, N. F., & Scambos, T. A. (2008). A structural glaciological analysis of the 2002 Larsen B ice-shelf collapse. *Journal of Glaciology*, *54*(184), 3–16. https://doi.org/10.3189/002214308784409017

Gorelick, N., Hancher, M., Dixon, M., Ilyushchenko, S., Thau, D., & Moore, R. (2017). Google Earth engine: Planetary-scale geospatial analysis for everyone. *Remote Sensing of Environment*, *202*, 18–27. https://doi.org/10.1016/j.rse.2017.06.031

Hock, R., de Woul, M., Radić, V., & Dyurgerov, M. (2009). Mountain glaciers and ice caps around Antarctica make a large sea-level rise contribution. *Geophysical Research Letters*, *36*, L07501. https://doi.org/10.1029/2008GL037020

Holland, P. R., Brisbourne, A., Corr, H. F. J., McGrath, D., Purdon, K., Paden, J., et al. (2015). Oceanic and atmospheric forcing of Larsen C ice-shelf thinning. *The Cryosphere*, *9*(3), 1005–1024. https://doi.org/10.5194/tc-9-1005-2015

Holland, P. R., Corr, H. F. J., Pritchard, H. D., Vaughan, D. G., Arthern, R. J., Jenkins, A., & Tedesco, M. (2011). The Air Content of Larsen Ice Shelf. *Geophysical Research Letters*, *38*, L10503. https://doi.org/10.1029/2011GL047245

King, J. C., Kirchgaessner, A., Bevan, S., Elvidge, A. D., Kuipers Munneke, P., Luckman, A., et al. (2017). The impact of Föhn winds on surface energy balance during the 2010–2011 melt season over Larsen C ice shelf, Antarctica: Föhn winds and Larsen C ice shelf. *Journal of Geophysical Research: Atmospheres*, *122*, 12,062–12,076. https://doi.org/10.1002/2017JD026809

Kuipers Munneke, P., Luckman, A. J., Bevan, S. L., Smeets, C. J. P. P., Gilbert, E., Broeke, M. R., et al. (2018). Intense winter surface melt on an Antarctic ice shelf. *Geophysical Research Letters*, *45*, 7615–7623. https://doi.org/10.1029/2018GL077899

Kuipers-Munneke, P., Ligtenberg, S. R. M., Van Den Broeke, M. R., & Vaughan, D. G. (2014). Firn air depletion as a precursor of Antarctic ice-shelf collapse. *Journal of Glaciology*, (220). https://doi.org/10.3189/2014JoG13J183

Kunz, M., King, M. A., Mills, J. P., Miller, P. E., Fox, A. J., Vaughan, D. G., & Marsh, S. H. (2012). Multi-Decadal Glacier Surface Lowering in the Antarctic Peninsula. *Geophysical Research Letters*, *39*, L19502. https://doi.org/10.1029/2012GL052823

Lorenz, E.N. (1956). Empirical orthogonal functions and statistical weather prediction, Science Report 1, Department of Meteorology, Massachusetts Institute of Technology.

Luckman, A., Elvidge, A., Jansen, D., Kulessa, B., Kuipers Munneke, P., King, J., & Barrand, N. E. (2014). Surface melt and ponding on Larsen C ice shelf and the impact of Föhn winds. *Antarctic Science*, *26*(06), 625–635. https://doi.org/10.1017/S0954102014000339

MacAyeal, D. R., & Sergienko, O. V. (2013). The flexural dynamics of melting ice shelves. *Annals of Glaciology*, *54*(63), 1–10. https://doi.org/10.3189/2013AoG63A256

Morris, E., & Vaughan, D. (2003). Spatial and Temporal Variation of Surface Temperature on the Antarctic Peninsula and the Limit of Viability of Ice Shelves. *Antarctic Research Series*, *79*, 61–68. https://doi.org/10.1029/AR079p0061

Mote, T., Anderson, M. R., Kuivinen, K. C., & Rowe, M. C. (1993). Passive microwave-derived spatial and temporal variations of summer melt on the Greenland ice sheet. *International Symposium On Remote Sensing of Snow and Ice*, *17*, 233–238.

Nagler, T., Rott, H., Ripper, E., Bippus, G., & Hetzenecker, M. (2016). Advancements for Snowmelt Monitoring by Means of Sentinel-1 SAR. *Remote Sensing*, *8*(4), 348. https://doi.org/10.3390/rs8040348

Pritchard, H. D., Ligtenberg, S. R. M., Fricker, H. A., Vaughan, D. G., van den Broeke, M. R., & Padman, L. (2012). Antarctic ice-sheet loss driven by basal melting of ice shelves. *Nature*, *484*(7395), 502–505. https://doi.org/10.1038/nature10968

Rott, H., Müller, F., Nagler, T., & Floricioiu, D. (2011). The imbalance of glaciers after disintegration of Larsen-B ice shelf, Antarctic peninsula. *The Cryosphere*, *5*(1). https://doi.org/10.5194/tc-5-125-2011

Rott, H., Rack, W., Nagler, T., & Skvarca, P. (1998). Climatically induced retreat and collapse of northern Larsen ice shelf, Antarctic peninsula. *Annals of Glaciology*, *27*, 86–92. https://doi.org/10.3189/S0260305500017262

Scambos, T., Hulbe, C., & Fahnestock, M. (2003). Climate-Induced Ice Shelf Disintegration in the Antarctic Peninsula. Antarctic Peninsula Climate Variability: Historical and Paleoenvironmental Perspectives. Washington, DC: American Geophysical Union. https://doi.org/10.1029/AR079p0079

Scambos, T. A., Bohlander, J. A., Shuman, C. A., & Skvarca, P. (2004). Glacier acceleration and thinning after ice shelf collapse in the Larsen B embayment, Antarctica. *Geophysical Research Letters*, *31*, L18402. https://doi.org/10.1029/2004GL020670

Scambos, T. A., Hulbe, C., Fahnestock, M., & Bohlander, J. (2000). The link between climate warming and break-up of ice shelves in the Antarctic peninsula. *Journal of Glaciology*, *46*(154), 516–530. https://doi.org/doi:10.3189/172756500781833043

Schannwell, C., Cornford, S., Pollard, D., & Barrand, N. E. (2018). Dynamic Response of Antarctic Peninsula Ice Sheet to Potential Collapse of Larsen C and George VI Ice Shelves. *The Cryosphere*, *12*(7), 2307–2326. https://doi.org/10.5194/tc-12-2307-2018

Shepherd, A., Wingham, D., Payne, T., & Skvarca, P. (2003). Larsen ice shelf has progressively thinned. *Science*, *302*(5646), 856–859. https://doi.org/10.1126/science.1089768

Small, D. (2011). Flattening gamma: Radiometric terrain correction for SAR imagery. *IEEE Transactions on Geoscience and Remote Sensing*, *49*(8), 3081–3093. https://doi.org/10.1109/TGRS.2011.2120616

Speirs, J. C., McGowan, H. A., Steinhoff, D. F., & Bromwich, D. H. (2013). Regional climate variability driven by Foehn winds in the McMurdo dry valleys, Antarctica. *International Journal of Climatology*, *33*(4), 945–958. https://doi.org/10.1002/joc.3481

Steinhoff, D. F., Bromwich, D. H., Speirs, J. C., McGowan, H. A., & Monaghan, A. J. (2014). Austral summer Foehn winds over the McMurdo dry valleys of Antarctica from polar WRF. *Quarterly Journal of the Royal Meteorological Society*, *140*(683), 1825–1837. https://doi.org/10.1002/qj.2278

Tedesco, M. (2007). Snowmelt detection over the Greenland ice sheet from SSM/I brightness temperature daily variations. *Geophysical Research Letters*, *34*, L02504. https://doi.org/10.1029/2006GL028466

Ulaby, F. T., & Stiles, W. H. (1980). The active and passive microwave response to snow parameters: 2. Water equivalent of dry snow. *Journal of Geophysical Research*, *85*, 1045–1049. https://doi.org/10.1029/JC085iC02p01045

van der Veen, C. J. (1998). Fracture mechanics approach to penetration of surface crevasses on glaciers. *Cold Regions Science and Technology*, *27*, 31–47. https://doi.org/10.1016/S0165-232X(97)00022-0,1998.TS73

Van Wessem, J. M., Reijmer, C. H., van de Berg, W. J., van den Broeke, M. R., Cook, A. J., van Ulft, L. H., & van Meijgaard, E. (2015). Temperature and wind climate of the Antarctic peninsula as simulated by a high-resolution regional atmospheric climate model. *Journal of Climate*, *28*, 7306–7326. https://doi.org/10.1175/JCLI-D-15-0060.1

Vaughan, D. G., & Doake, C. S. M. (1996). Recent atmospheric warming and retreat of ice shelves on the Antarctic peninsula. *Nature*, *379*(6563), 328–331. https://doi.org/10.1038/379328a0

Weertman, J. (1973). *Can a water-filled crevasse reach the bottom surface of a glacier* (Vol. 95, pp. 139–145). Oxfordshire, UK: IASH Publications.

Wiesenekker, J., Kuipers Munneke, P., van den Broeke, M., & Smeets, C. (2018). A multidecadal analysis of Föhn winds over Larsen C ice shelf from a combination of observations and modeling. *Atmosphere*, *9*(5), 172. https://doi.org/10.3390/atmos9050172

Wilks, D. S. (1995). *Statistical methods in the atmospheric sciences: An introduction, international geophysics*. Amsterdam, Netherlands: Elsevier Science.

Zwally, H. J., & Fiegles, S. (1994). Extent and Duration of Antarctic Surface Melting. *Journal of Glaciology*, *40*, 463–476. https://doi.org/10.1017/S0022143000012338